Immunity, Volume *54*

Supplemental information

Deep spatial profiling of human COVID-19 brains reveals neuroinflammation with distinct microanatomical microglia-T-cell interactions

Marius Schwabenland, Henrike Salié, Jovan Tanevski, Saskia Killmer, Marilyn Salvat Lago, Alexandra Emilia Schlaak, Lena Mayer, Jakob Matschke, Klaus Püschel, Antonia Fitzek, Benjamin Ondruschka, Henrik E. Mei, Tobias Boettler, Christoph Neumann-Haefelin, Maike Hofmann, Angele Breithaupt, Nafiye Genc, Christine Stadelmann, Julio Saez-Rodriguez, Peter Bronsert, Klaus-Peter Knobeloch, Thomas Blank, Robert Thimme, Markus Glatzel, Marco Prinz, and Bertram Bengsch

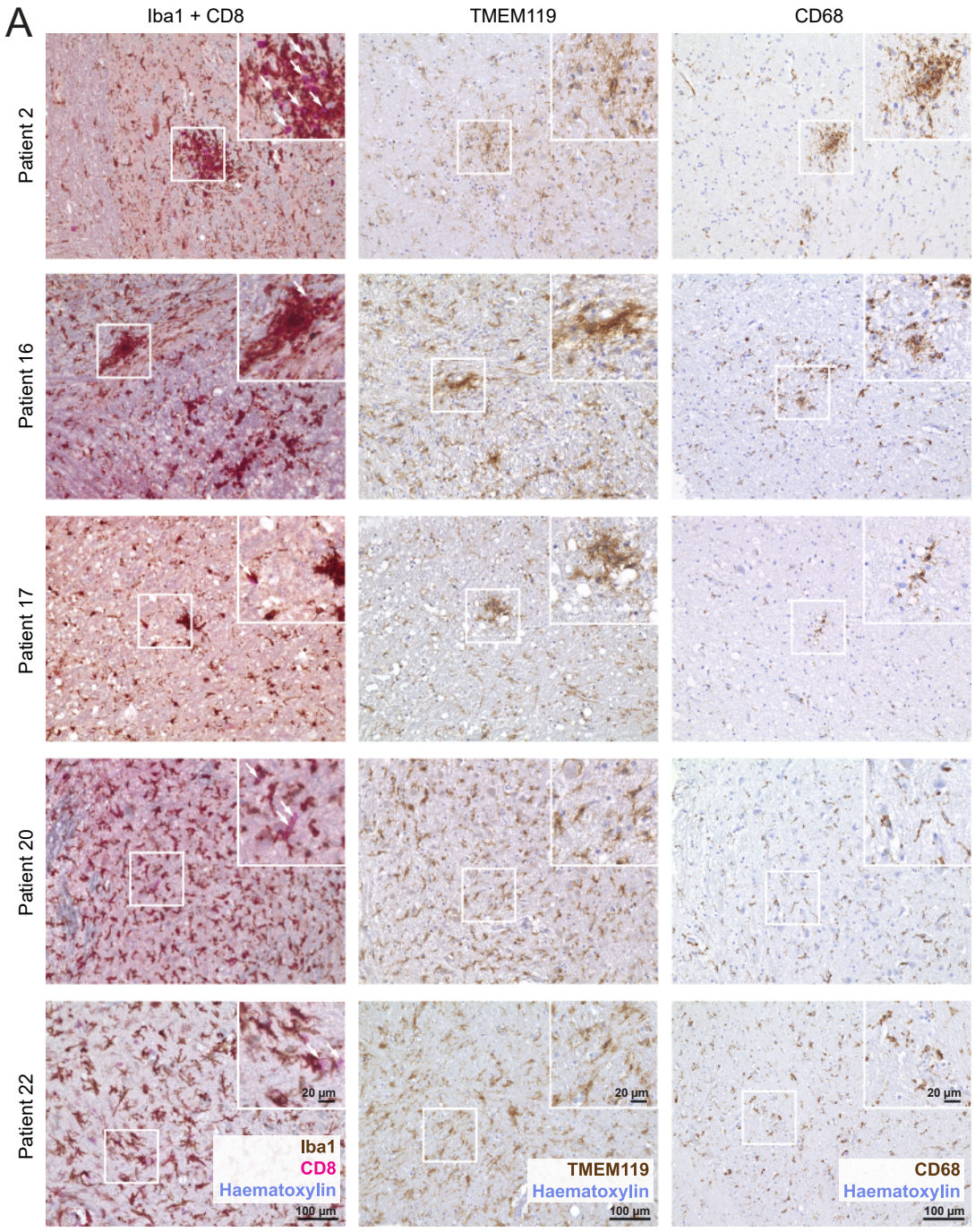

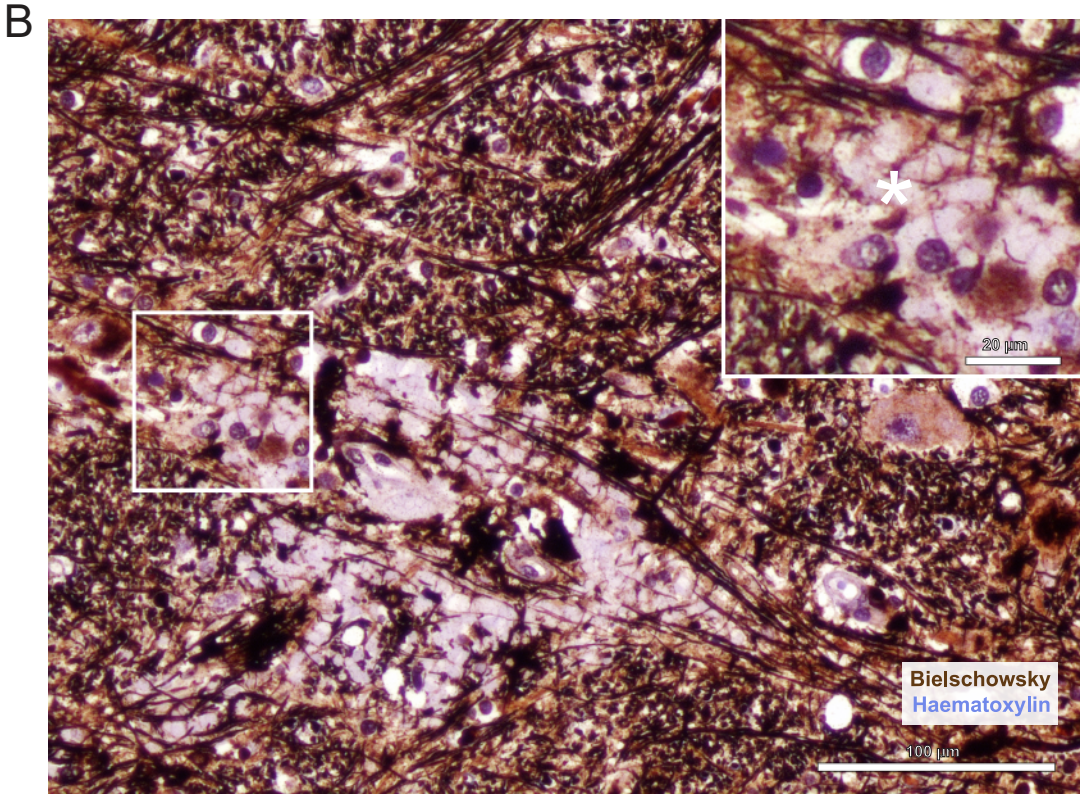

Supplementary Fig. 1

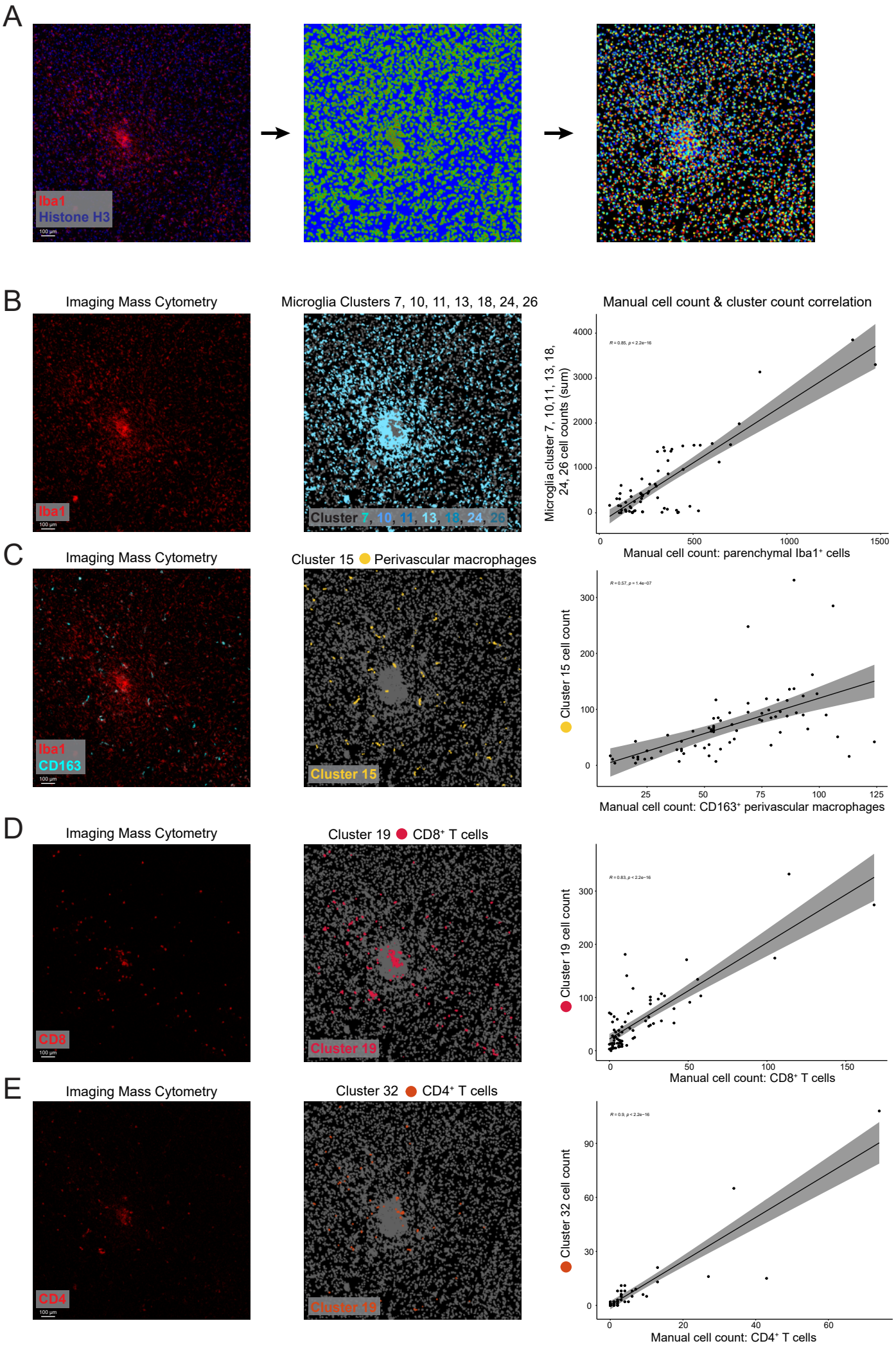

Supplementary Fig. 2

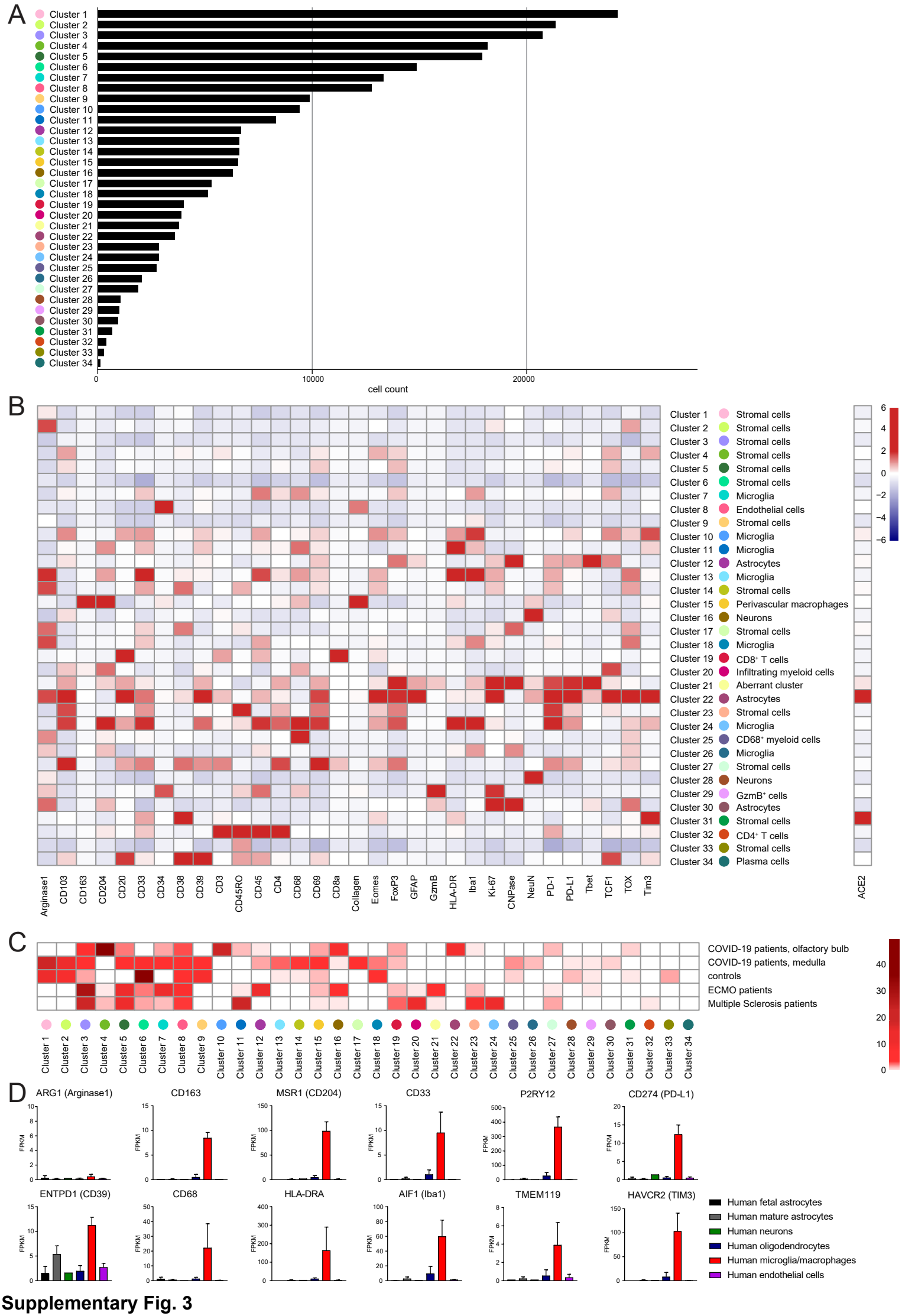

Supplementary Fig. 3

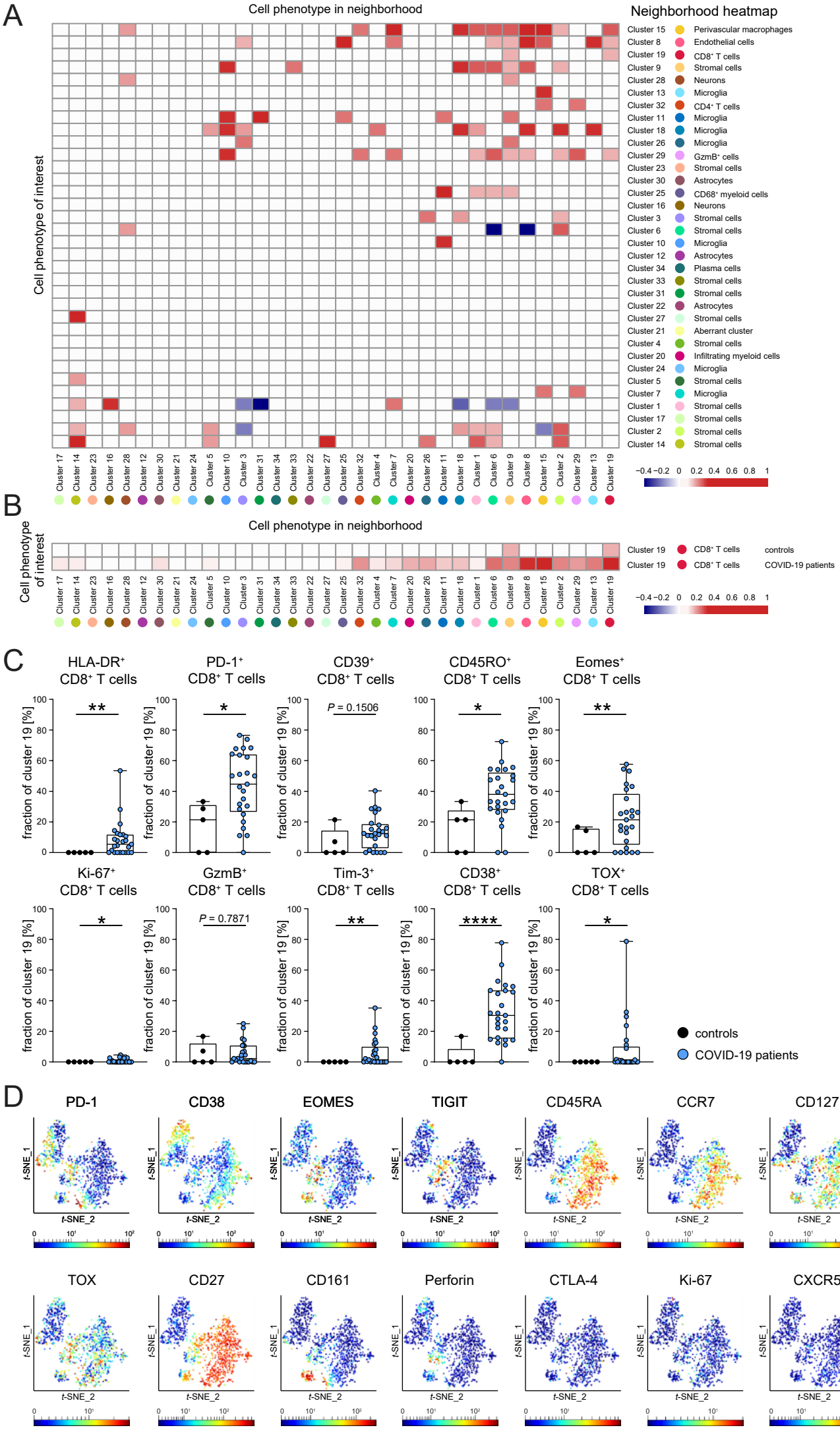

Supplementary Fig. 4

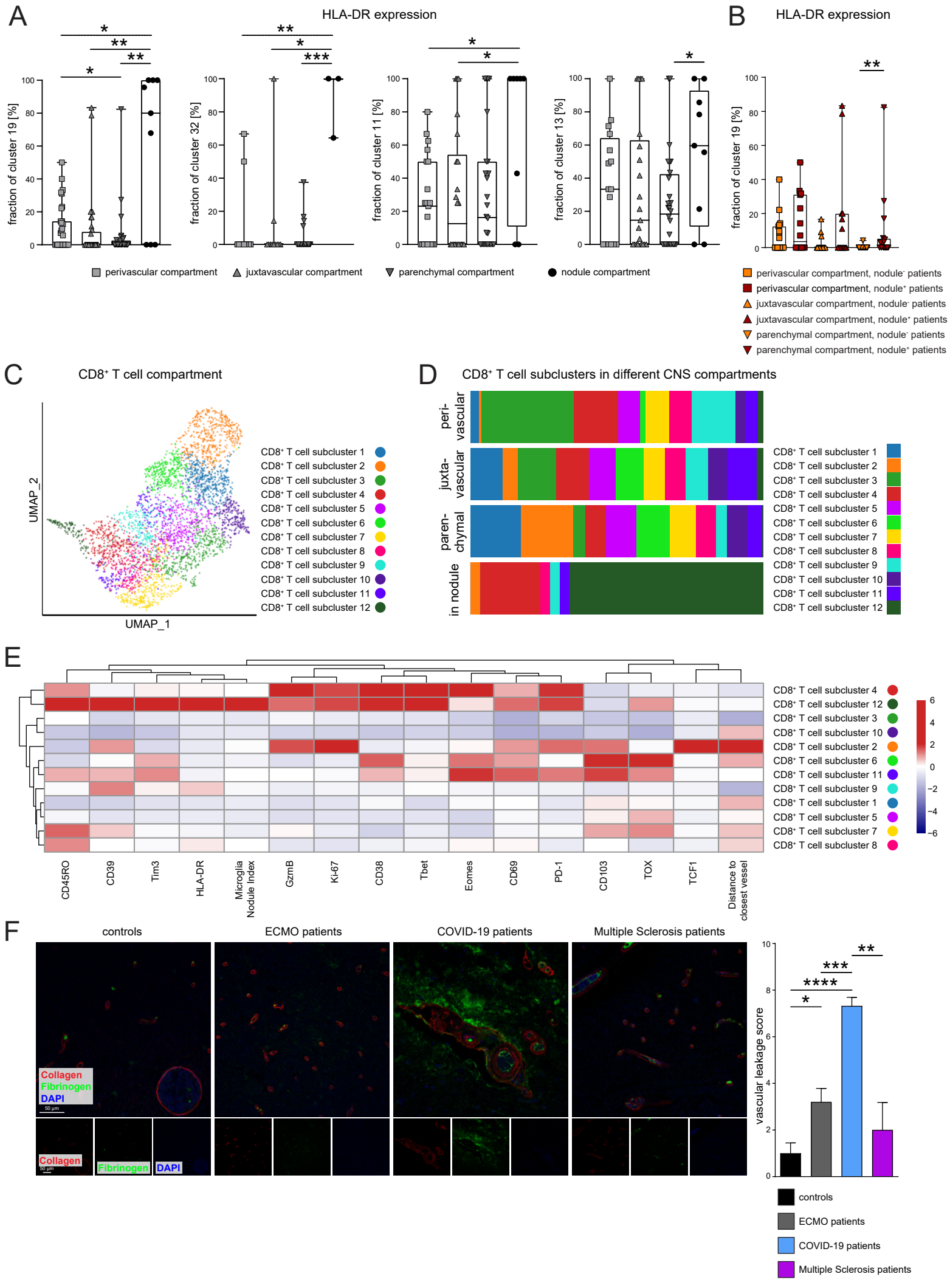

Supplementary Fig. 5

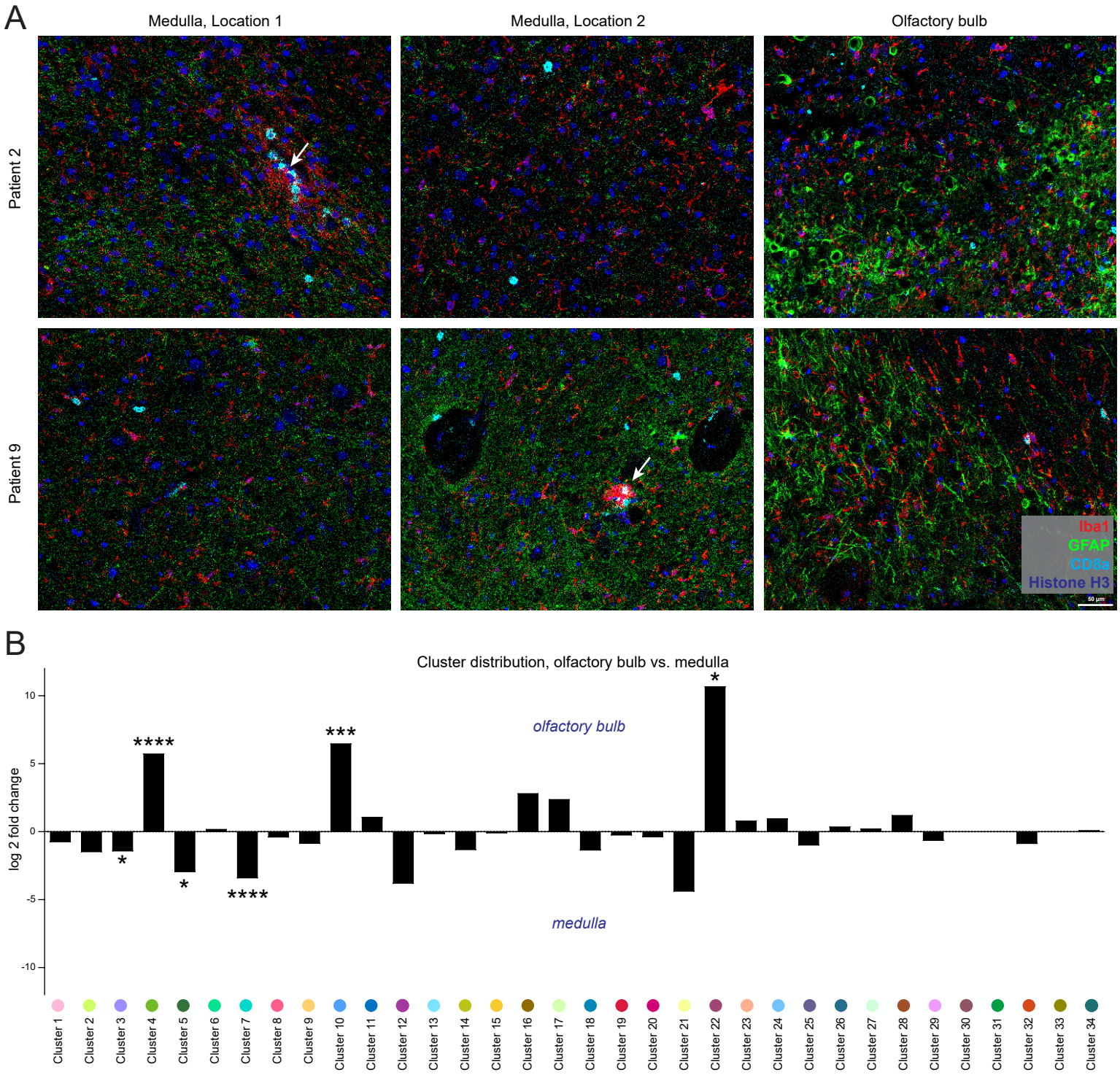

Supplementary Fig. 6

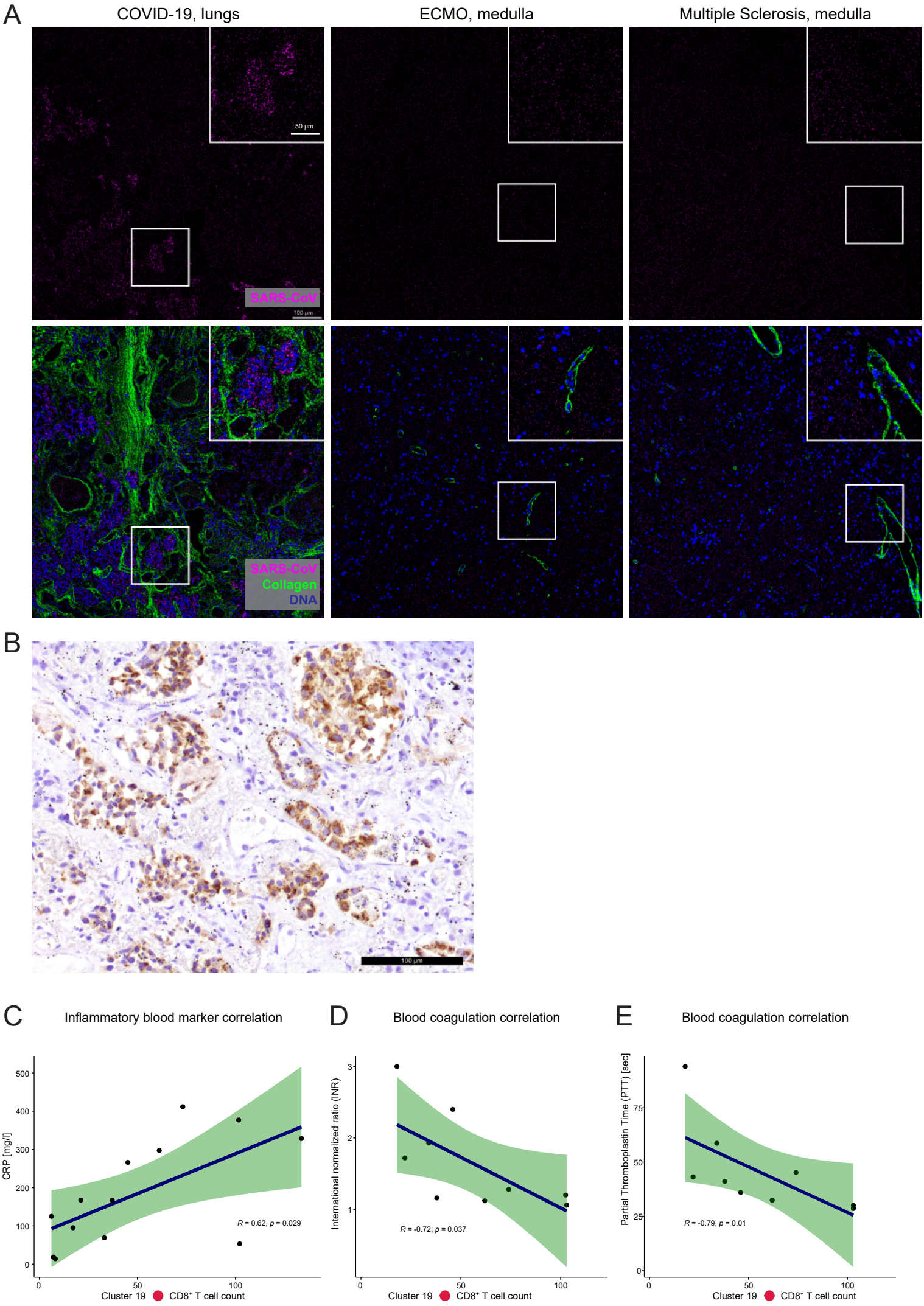

Supplementary Fig. 7

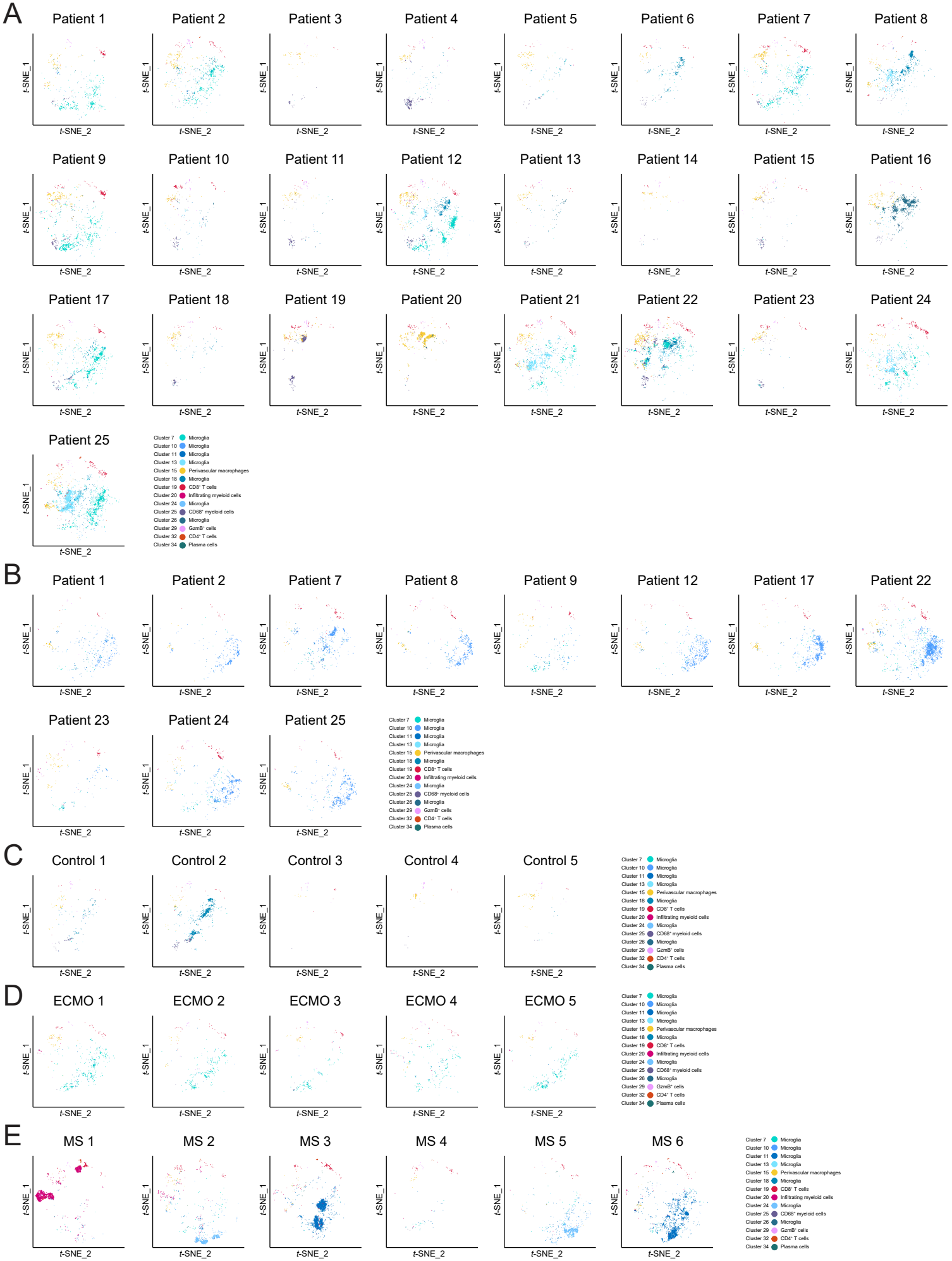
A
Patient 1
Patient 2
Patient 3
Patient 4
Patient 5
Patient 6
Patient 7
Patient 8
Patient 9
Patient 10
Patient 11
Patient 12
Patient 13
Patient 14
Patient 15
Patient 16
Patient 17
Patient 18
Patient 19
Patient 20
Patient 21
Patient 22
Patient 23
Patient 24
Patient 25
t-SNE_1
t-SNE_2
Cluster 7 Microglia
Cluster 10 Microglia
Cluster 11 Microglia
Cluster 13 Microglia
Cluster 15 Perivascular macrophages
Cluster 18 Microglia
Cluster 19 CD8⁺ T cells
Cluster 20 Infiltrating myeloid cells
Cluster 24 Microglia
Cluster 25 CD68⁺ myeloid cells
Cluster 26 Microglia
Cluster 29 GzmB⁺ cells
Cluster 32 CD4⁺ T cells
Cluster 34 Plasma cells
B
Patient 1
Patient 2
Patient 7
Patient 8
Patient 9
Patient 12
Patient 17
Patient 22
Patient 23
Patient 24
Patient 25
C
Control 1
Control 2
Control 3
Control 4
Control 5
D
ECMO 1
ECMO 2
ECMO 3
ECMO 4
ECMO 5
E
MS 1
MS 2
MS 3
MS 4
MS 5
MS 6

Data S1

SUPPLEMENTARY FIGURE LEGENDS

Supplementary figure 1 related to Figure 1: Immunohistochemistry for microglial markers and Bielschowsky stain indicates microgliosis, microglial nodules and neuronal injury.

A: Immunohistochemistry for Iba1 (brown) combined with CD8 (magenta), TMEM119 (brown) and CD68 (brown) is shown. The samples were counterstained with Haematoxylin (blue). Arrows point towards CD8-positive T cells in magenta. Scale bar represent 100 µm and 20 µm in the inserts.

B: Bielschowsky stain. A representative image showing a loss of continuous black staining at a site of myeloid accumulation, indicating axonal rarefication (asterisks). The scale bar represents 100 µm and 20 µm in the insert.

Supplementary figure 2 related to Figure 2: Cell annotation by single-cell segmentation and clustering correlates with manual inspection.

A: Representative visualization depicting an original IMC image (with Iba1 staining indicated in red and histone H3 in blue)(left), probabilities for nucleus (red), cytoplasm (green) and background (blue) categories calculated in Ilastik (middle) and combined probabilities and microglia cell mask as created in CellProfiler (right).
B-E: Depiction of the key markers on the raw image (left) and corresponding cluster masks for the designated populations (middle) and correlations with manual counted populations (right) are shown for microglia clusters (B), perivascular macrophages (C), CD8 T cells (D), CD4 T cells (E).

Supplementary figure 3 related to Figure 2: Abundance and molecular expression patterns of high-dimensional clusters.

A: Bar graph visualizing cell counts of Phenograph clusters. Clusters are enumerated based on abundance of a given cluster in the combined analysis of all tissue samples.

B: Median marker expression of Phenograph clusters shown in a z-score normalized heatmap. ACE2 staining in the extension panel is shown on the right side.

C: Heatmap of the cluster distribution across patient groups and anatomic sites. Coloring indicates mean percentages as shown.

D: Cell-type-specific RNA expression levels of genes encoding for proteins depicted in Figure 2C were extracted from www.brainrnaseq.org and visualized across populations of astrocytes, neurons, microglia/macrophages, oligodendrocytes and endothelial cells (Zhang et al., 2016).

Supplementary figure 4 related to Figure 3: Cellular neighborhood analysis and mass cytometry profiling reveal context-specific T cell interaction partners as well as differential activation and exhaustion signatures.

A: Heatmap depicting results of the neighborhood analysis in control patients similar to the analysis in COVID-19 patients described in Figure 3B. The cluster order on both axis was chosen according to Figure 3B to facilitate comparison.

B: Cluster c19 spatial neighborhood interactions were determined in COVID-19 and control patients. Rows indicate significant enrichment or depletion of cells from clusters c1 - c34 in the vicinity of c19 cells.

C: Cluster c19 cells were analyzed for expression of immune markers involved in T-cell activation, differentiation, exhaustion and function. Frequency of positive cells is shown as boxplots with median, IQR and upper and lower whiskers and compared between patient groups.

D: CD8 T cells isolated from the medulla, olfactory bulb, cortex and regional lymph node of a deceased COVID-19 patient were analyzed by suspension mode mass cytometry as in Fig. 3F. CD8 T cells are visualized on a tSNE map. The expression of several exhaustion markers is indicated by heatmap coloring.

Significant differences were determined by unpaired *t* tests with Welch's correction in C.

Supplementary figure 5 related to Figure 5: Immune activation and T cell subsets differ between the brain's perivascular, juxtavascular, perivascular and nodule compartment and is associated with vascular disintegrity.

A: HLA-DR expression of CD8 T cells, CD4 T cells and activated microglial cells in different CNS compartments. A: Frequencies of HLA-DR$^+$ cells of cluster c19 CD8 T cells, c32 CD4 T cells, c11 and c13 microglia are compared across perivascular, juxtavascular, parenchymal and nodule compartments.

B: HLA-DR expression by cluster c19 CD8 T cells in anatomic compartments depending on presence of microglial nodules in the sample.

C: Cluster c19 cells were subclustered based on informative markers and visualized using a UMAP analysis.

D: Distribution of CD8 T cell subclusters in anatomical compartments is shown by stacked bar plot.

E: Heatmap with hierarchical clustering informing about the phenotype and indices of anatomical compartments of CD8 subclusters. Heatmap indicates z-scores.

F: Vascular leakage was determined by immunofluorescence analysis of fibrinogen (green) together with collagen (red) and DAPI (blue) stain across the patient cohorts. Representative stainings per group are shown and a summary of the vascular leakage score is provided as a bar graph +/- SEM. Significant differences were determined by Mann-Whitney-U tests in A and B.

Supplementary Figure 6 related to Figure 7: Comparison of the cellular profile in local and distant brain stem and olfactory bulb sections reveals core immune patterns but also region-specific differences in immune and astrocyte subtypes.

A: Comparison of IMC stainings across different CNS locations. Stainings were performed on sections obtained from the medulla (2 locations) and one section obtained from the olfactory bulb in 11 COVID-19 patients. Stainings from two exemplary patients are shown (left to right: medulla location 1, medulla location 2 and olfactory bulb). Visualization of Iba1 (red), GFAP (green) CD8 (turquoise) and histone H3 (blue). Scale bar indicates 50 µm. White arrows indicate nodules.

B: Differences of cluster composition in the olfactory bulb and medulla are visualized by enrichment of clusters. The ratio between the area-normalized mean cluster counts in the olfactory bulb and the mean cluster counts in the medulla is visualized on a log2 scale.

C: Prevalence of microglial nodules in the olfactory bulb and medulla based on IMC analysis or larger area high-throughput IHC analysis.

D: Astrogliosis assessment between CNS localizations. Left: Fractions of GFAP$^+$ pixels of the ROIs are compared between the olfactory bulb and medulla of COVID-19 patients. Right: Comparison of mean signal intensity (MSI) between astrocyte clusters c12 and c22.

E: Comparison of the frequency of ACE$^+$ cells in cluster c12 and c22.

Significant differences were determined by unpaired *t* tests with Welch's correction in B, Mann-Whitney U test in D (left), and Wilcoxon signed-rank test in D (right) and E.

Supplementary figure 7 related to Figure 7: SARS-CoV-spike protein is detected by IMC in the lung of COVID-19 patients but not in controls and specific brain immune clusters correlate with clinical measures in COVID-19.

A: Representative IMC images showing positive SARS-CoV spike protein antibody staining in the lung of a COVID-19 patient and negative staining in the medulla of ECMO and MS patients. Shown are channels for SARS-CoV spike protein (pink), Collagen (green) and DNA (blue). Scale bars indicate 100µm in the image and 50µm in the inserts respectively.

B: Immunohistochemistry staining of SARS-CoV spike protein (brown) in the lung of a COVID-19 patient. Counterstaining with hematoxylin. Scale bar indicates 100 µm.

C-E: Correlation of cluster 19 counts with CRP, INR and PTT were performed. R and p values were determined by spearman correlation. The correlation is indicated by the line, dots represent individual patients.

Data S1 related to Figure 2: Brain immune maps are visualized via tSNE per patient and brain region.

The *t*-SNE visualization of the brain immune landscape as in Figure 2D is shown for individual patients. Brain immune maps are shown from the (A) medulla and (B) olfactory bulb of COVID-19 patients, and the medulla of (C) control patients, (D) ECMO patients and (E) Multiple Sclerosis patients. Each dot represents a cell. The coloring refers to the respective immune cell cluster as indicated.